Int. J. Electrochem. Sci., 15 **(2020)** 4988 – 5001, doi: 10.20964/2020.06.17

International Journal of
ELECTROCHEMICAL
SCIENCE
www.electrochemsci.org

Short Communication

Study on Electrochemical Behavior of 20# Carbon Steel with Disbonded Coating by Scanning Kelvin Probe and Local Electrochemical Impedance Spectroscopy

Changyou Wang[1,2], *Yanmei Li*[2], *Lucia Alvarado*[2]

[1] Chongqing University of Science and Technology, 401331, Chongqing, P. R. China.
[2] Department of Engineering, University of Guanajuato, 36000, Mexico
[*]E-mail: wcybodao@126.com

Received: 9 February 2020 / *Accepted:* 27 March 2020 / *Published:* 10 May 2020

As oil & gas pipelines are built underneath the earth's surface, corrosion-protecting coatings may produce different kinds of defects that cause from many kinds of factors underneath the soil. After a break or disband occurs in the pipeline coating, crevices form between the coating and the metallic substrate. Corrosive dielectric forms at the crevice and causes crevice corrosion to occur on the metallic substrate. Even worse, crevice corrosion lowers the protective effect of the coating and shortens the life of pipelines; the corrosion can even lead to exploding after the pipelines have perforation leakage. This paper adopted a simulation experiment and theoretical analysis, and promoted the micro-electrochemical behavior associated with the crevice corrosion of pipelines; tests were conducted with coatings containing different defect sizes to study the local corrosion mechanism at the crevice.

Keywords: 20# Carbon Steel; Scanning Kelvin Probe (SKP); Local Electrochemical Impedance Spectroscopy (LEIS); Crevice corrosion

1. INTRODUCTION

In 1987, Stratmann [1] applied SKP technology to corrosion research for the first time and it was used to study the peeling behavior of organic coatings and found the foaming phenomenon of coatings in the initial stage of corrosion. The results show that the stripping behavior of the carbon steel coating is controlled by a cathodic stripping mechanism. As the cathode of the corrosion reaction, the stripping front mainly occurs in the oxygen reduction reaction, which leads to an increase in alkalinity. Additionally, an increase in the destructive ion content weakens the bonding force between the metal and the coating, which leads to the stripping of the coating. Sheng [2] studied the electrochemical characteristics and corrosion behavior of 2024-T351 high strength aluminium alloy crack tips in a 3.5%NaCl solution by combining SKP with a capillary microelectrode test method. The results show

that the corrosion potential at the crack tip is more negative than that of the matrix far away from the crack tip, and the electrochemical activity at the crack tip has an obvious increasing trend. Nazarov [3] studied the corrosion of zinc/polymer surfaces by combining SKP with EIS technologies. The SKP measurement results show that when water enters the joint of the coating and the substrate, the local bonding force decreases and the corrosion surface becomes inhomogeneous. Furbeth [4] studied the effect of zinc coating damage on the coating peeling mechanism and found that if the zinc coating is intact and undamaged, the stripping of the coating is controlled by the cathodic stripping mechanism; if the zinc coating has been damaged, the stripping of the coating is controlled by the combination of anodic dissolution and cathodic stripping. Initially, it is cathodic stripping. When stripping occurs, zinc is exposed in the electrolyte at the interface, and anodic dissolution occurs, that is, the zinc acts as sacrificial anode protection that is alternately controlled. Doherty [5] also used SKP technology to study a chrome-plated steel/epoxy phenolic resin finish system immersed in NaCl (concentration of 0.17mol/L). By monitoring the potential changes in different stages and comparing with other test results such as EIS, they found that the defects at the initial stage of immersion were used as anodes, and the adjacent area under the membrane was the cathode, which resulted in the oxygen reduction reaction. Yang [6] investigated inhibition effect of ketoconazole on mild steel corrosion in Hydrochloric acid by SKP and found that at the period of contact the potential of the mild steel tends to be irregular without Ketoconazole due to the commencement of deterioration causing fractures and fissures on the surface. Yi [7] investigated corrosion behavior of printed circuit board and hot air solder levelling during marine environment of industrial pollution with SKP and found that in the aspect of thermodynamics, Kelvin surface potential of the specimens gradually increased, large cracks and exposed “fresh” substrate (Cu) must be responsible for reducing of Kelvin potential. Later, corrosion of substrate contributed to increasing of Kelvin surface potential at 12m. Jiang [8] applied SKP and SEM to study the effect of precipitated phases on corrosion behavior of Mg-Y-Nd ternary alloy and found that Mg_3(Y, Nd) and Mg_{12}(Y, Nd) phases served as the cathode of the electrochemical reaction to accelerate the corrosion of the α-Mg matrix.

Zhong [9] used LEIS to study the local corrosion behavior of steel with a defect coating in a near neutral solution with LEIS. The results show that the metal corrosion under the coating is related to the defect size, and when the defect size is small, the corrosion reaction is mainly controlled by a diffusion process due to the blocking effect of the corrosion products; when the defect size is large, the blocking effect of the corrosion products is not obvious. Zou [10] used LEIS to study the local foaming behavior of epoxy coatings on carbon steel surfaces. It was found that LEIS can effectively obtain information on water penetration in the coating by measuring the coating capacitance around the foaming area. Dong [11] studied the influence of cathodic protection on the local electrochemical activity of the 3LPE anticorrosive coating defects of X65 pipeline steel. Through the electrochemical impedance information of the micro-area under -800mV and -1200mV cathodic protection potentials, it is found that the more negative the cathodic protection potential is, the greater the impedance value at the same location. This shows that the cathodic protection potential affects the corrosion behavior of the coating steel with defects. The initiation and expansion information of coating delamination is clearly obtained by Jorcin [12] by applying LEIS. The research shows that the accumulation of corrosion products and the diffusion of oxygen play an important role in the process of delamination and expansion. Hang [13] combined

LEIS technology with MMT and ATMP technology to study the corrosion protection of an epoxy containing modified organic clay on medium carbon steel. The results show that the anti-corrosion effect of the epoxy resin mixed with the modified clay is obviously improved. Dehri [14] found that LEIS could only respond to the impedance within a certain distance from the cutting edge. Beyond this distance, the conductivity of the system is affected due to the large coating impedance. Information on the initiation and extension of coating delamination was clearly obtained by Jorcin [12] by applying LEIS. The results show that the accumulation of corrosion products and oxygen diffusion play an important role in the process of exfoliation. Zhou [15] researched corrosion behavior of Al_2Cu intermetallic compound and coupled Al_2Cu/Al with LEIS and found that the Al_2Cu region in coupled Al_2Cu/Al immersed in a solution is more difficult to dissolve relative to pure Al. Losiewicz [16] researched the effect of hydrogen electrosorption on corrosion resistance of $Pd_{80}Rh_{20}$ alloy in sulfuric acid by LEIS and EIS and found that local impedance lower than bulk impedance determined by EIS due to internal stresses and microcracks. Wang [17] investigated local electrochemical impedance and current distribution of scratches of MAO coated 7075 aluminum alloy with LEIS and SVET and discovered that with change of time, the minimum impedance value of the scratch decreases first and then increases from the third hour.

Currently, advanced micro-electrochemical measuring methods which are conducted by scanning Kelvin probe (SKP) and localized electrochemical impedance spectroscopy (LEIS) techniques, are being given more attention. These two methods can obtain local corrosion information from a microscopic perspective, thus revealing the whole process and mechanism of pipeline corrosion; furthermore, these techniques can provide the electrochemical corrosion parameters and information to offer basic data for underground pipeline protection. However, there are limited studies directly illustrated how defect sizes affect the corrosion behavior. This paper focused on revealing the whole process and mechanism of pipeline corrosion and obtaining the micro-electrochemical corrosion parameters and information of the pipelines for the underground pipelines protection.

2. EXPERIMENTAL

2.1. Materials and Solution

The working sample used for the measurement was cut from a 20# carbon steel pipe with the chemical composition shown in Table 1. The area of the sample was $1\times1cm^2$. The sample was put it into anhydrous ethanol, and then it was ground to 1500# with crystal sandpaper. Next, the sample was sealed with epoxy resin and put it into anhydrous ethanol after drying. The sample was cleaned with ultrasonic for 30s, and then dry for use. Rust removal, oxide scale removal and edge smoothing must be carried out before all samples are sealed. The metallographic structure of the 20# carbon steel used in the experiment is shown in Figure 1. It can be found that metallographic structure is not evenly distributed, and its metallographic microstructure at room temperature is mainly composed of grey white ferrite and black pearlite.

The deionized water is used to prepare soil simulated solution which contains 0.004mol NaCl + 0.02mol Na_2SO_4 + 0.001mol HCO_3, and the simulated solution was adjusted to pH=7.2 with deionized water. All the experiment samples were immersed in simulated solution for 10 days.

Table 1. Ingredients of 20# carbon steel sample used in the experiment

Chemical Composition	C	Si	Mn	S	P	Cr	Ni	Cu	Fe
（Wt%）	0.17-0.24	0.17-0.34	0.35-0.65	0.035	0.035	0.25	0.25	0.25	Rest

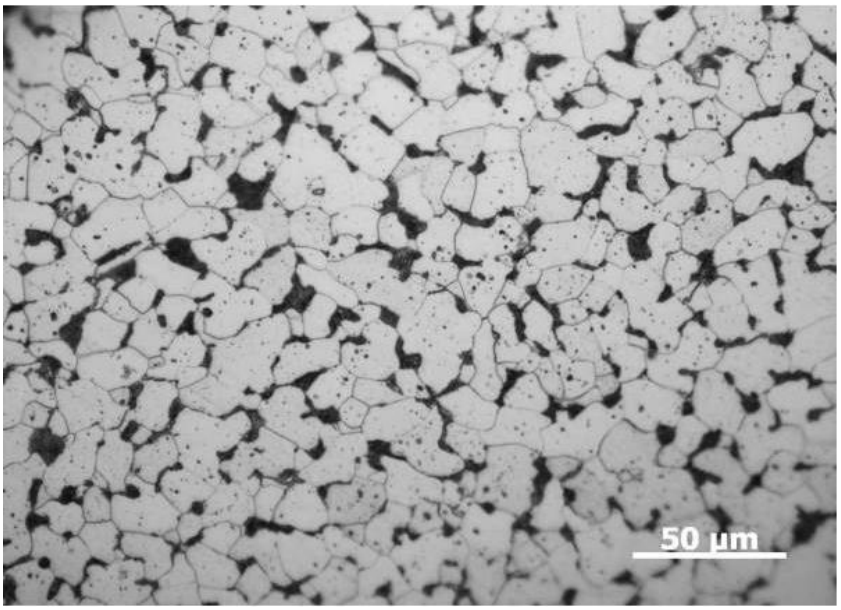

Figure 1. Metallurgical microstructure of 20# carbon steel sample at room temperature

2.2 Measurement

2.2.1 SKP measurement

The measurement of the Scanning Kelvin probe (SKP) was carried out on Versa SCAN workstation. The samples with coating defects soaked in simulated solution were removed, dried and placed on a tray. After fine levelling (the height difference between the front and back of the probe tip and the left and right ends within the scanning range was within 2μm), the samples were tested by surface scanning mode at different defect sizes. An electrolytically thinned tungsten wire was used as the probe with the following parameters: the diameter of the probe was 500μm, the periphery of the probe was shielded by a copper tube, the probe moved above the sample along a perpendicular direction perpendicular to the sample, the vibration amplitude was 30μm, the vibration frequency was fixed at 100Hz, and the distance between the probe and sample was kept at approximately 100μm. The scanning area was set with the defect as the positive center to ensure that the defect was in the middle of the scanning area. The scanning area of the defect with the width of 200μm was 1000μm ×1000μm; the scanning area of the defect with the width of 800μm was 2000μm ×2000μm. The probe scanned in the direction parallel to the line defect on the sample and automatically scanned to the next line after each line was scanned. The experiment was carried out at room temperature.

2.2.2 LEIS measurement

The measurement of the Local Electrochemical Impedance Spectroscopy (LEIS) was carried out on Princeton 370 micro area electrochemical workstation. A three-electrodes system was applied. The working electrode was a 20# carbon steel sample, the auxiliary electrode was a platinum probe, and the reference electrode was a saturated calomel electrode. The scanning mode was surface scanning. The distance between the probe tip and sample surface was approximately 100μm. The probe was adjusted and monitored by a microscope with a long focal length microscope combined with a real-time video camera system. The scanning frequency was fixed at 10000Hz, which was used to collect the impedance modulus information at different scanning positions to monitor the corrosion state of the micro area near the metal/coating interface. The scanning area of the defect with the width of 200μm was 1000μm ×1000μm; the scanning area of the defect with the width of 800μm was 2000μm ×2000μm. The test was carried out at the open circuit potential and at room temperature. Because the measurement of the micro-area impedance was easily affected by the external environment, electromagnetic shielding was applied to the measurement system during the measurement process to minimize the interference of external factors on the experiment.

3. RESULTS AND DISCUSSION

3.1 SKP measurement results and discussion

Figure 2 is the SKP measurement diagrams of 20# carbon steel samples with defect sizes of 200μm and 800μm widths after immersing in simulated solution for 10 days.

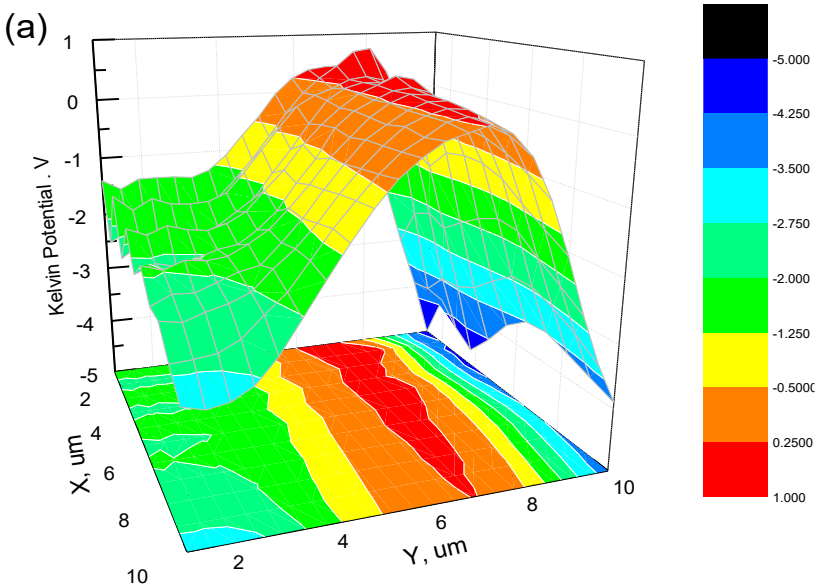

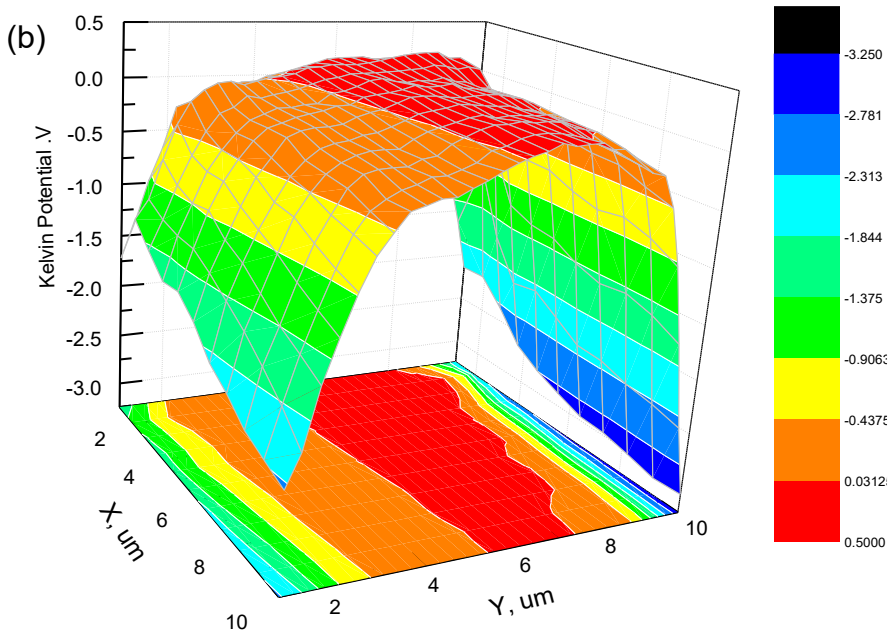

Figure 2. SKP measurement diagrams of 20# carbon steel samples with different defect sizes after immersing in simulated solution for 10 days: (a) 200μm and (b) 800μm

In the figure, the x-axis and y-axis are the scanning positions of the probe (the same in the LEIS measurement), and the z-axis is the potential at the scanning position. It can be seen from the figure that as the probe moves from the intact part of the coating to the defective part, the potential on the surface of the sample increases gradually and reaches its highest value at the defective part of the coating. The maximum potential at the defect of the 200μm width coating is approximately 0.2500V. The potential of the 800μm width coating defect is approximately 0.0125V, the former potential value is higher than the latter, and the high potential area of the 800 μm width coating defect is larger than that of the 200μm width coating defect, which corresponds to their physical dimensions.

According to the measurement principle of the Scanning Kelvin probe, it can be found that is a linear relationship between the corrosion potential and Kelvin potential of the metal as following:

$$E_{corr}=\alpha+bE_{kp} \quad (1)$$

The highest potential (E_{kpmax}) and the lowest potential (E_{kpmin}) of the measurement system correspond to the cathode potential and anode potential of the reaction system respectively.

In this paper, the defects of the coating are covered by a rust layer, and electrons must overcome a series of potential barriers to migrate. Taking the coating defect as an example, the electrons escape through the interface of the metal matrix defect coating, the rust and air. The actual measured electron work equation is as following:

$$\frac{\varphi_{EXP}}{e}=\frac{\varphi_M}{e}+\beta_1+\beta_2+\beta_3=\frac{\varphi_M}{e}+\frac{q_1}{C_1}+\frac{q_2}{C_2}+\frac{q_3}{C_3} \quad (2)$$

Where β_1, $\beta_2$and β_3 are the potential differences of the three interfaces, q_1, q_2 and q_3 are the charges of the three interfaces, and C_1, C_2 and C_3 are the capacitance of the three interfaces [18]. From the SKP measurement results, with the increase in the width of the coating defect, the overall potential at the defect shifts negatively, and the surface potential gradually tends to be uneven. The results show that on one hand, under the action of the micro-area corrosion cell, it provides a driving force for the

reaction; on the other hand, under the coupling action of the positive and negative pole reactions, the overall potential of the coating defect decreases [19], resulting in the potential of the 200μm width defect being higher than that of the 800μm width defect.

Figure 3 and Figure 4 are the macro and local-enlarged corrosion morphologies of 20# carbon steel samples with defect sizes of 200μm and 800μm after immersing in simulated solution for 10 days, respectively. It can be seen from Figure 3 that there are less corrosion productions at the defects of the 200μm width and they are scattered; additionally, the corrosion product film does not completely cover the defects. However, at the defect of the 800μm width, the corrosion product film is dense and uniform. This is because the reaction system is closed at the defect of the coating with a width of 200μm, and the corrosive ions in the 20# carbon steel substrate and the solution did not react fully, thus resulting in a small amount of corrosion products generated after the reaction. At the defects of the coating with the width of 800μm, the reaction system is open, and the corrosive ions in the 20# steel substrate and the solution fully react, forming a corrosion production film that covers access to the defect.

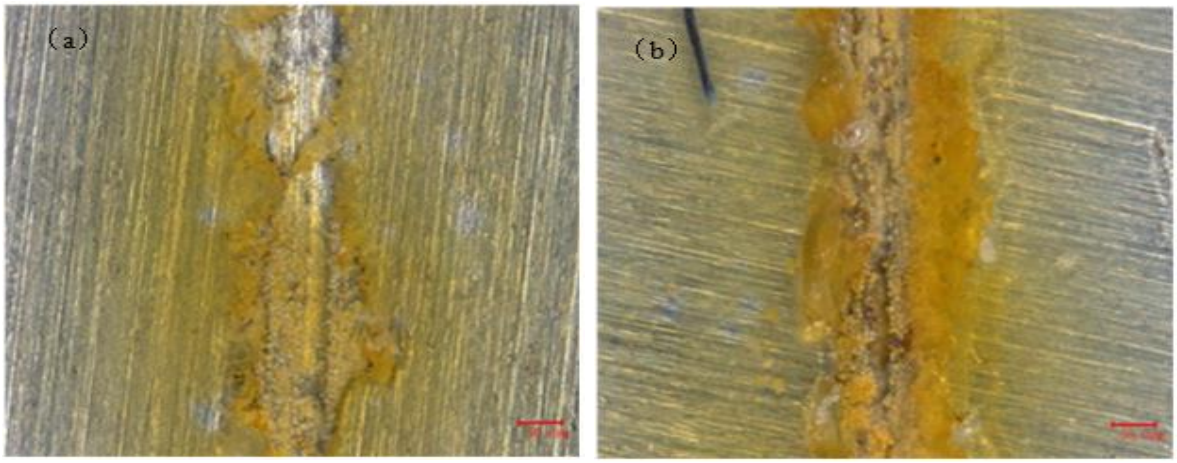

Figure 3. Macro corrosion morphologies of the 20# carbon steel samples with different defect sizes after immersing in simulated solution for 10 days: (a)200μm and (b)800μm

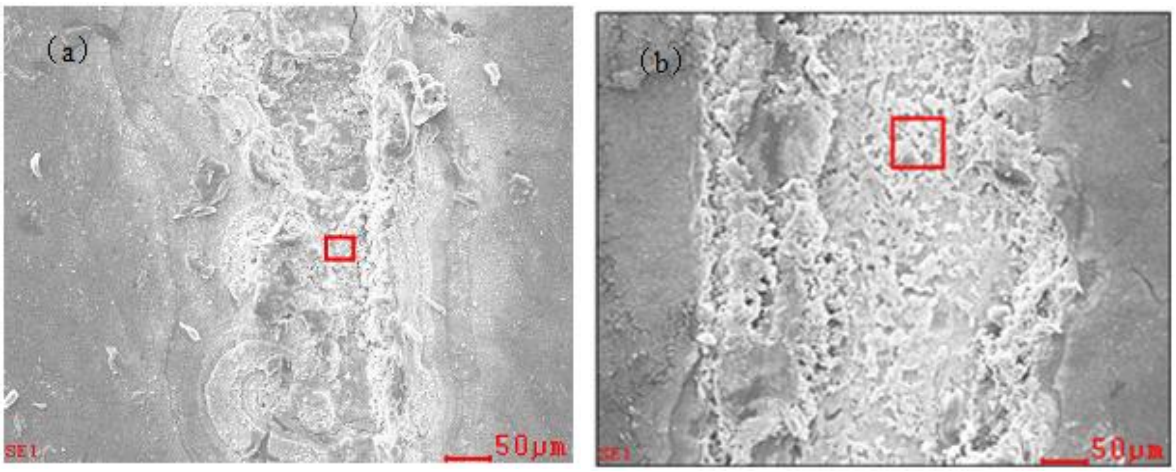

Figure 4. Local-enlarged corrosion morphologies of the 20# carbon steel samples with different defect sizes after immersing in simulated solution for 10 days: (a) 200μm and (b) 800μm

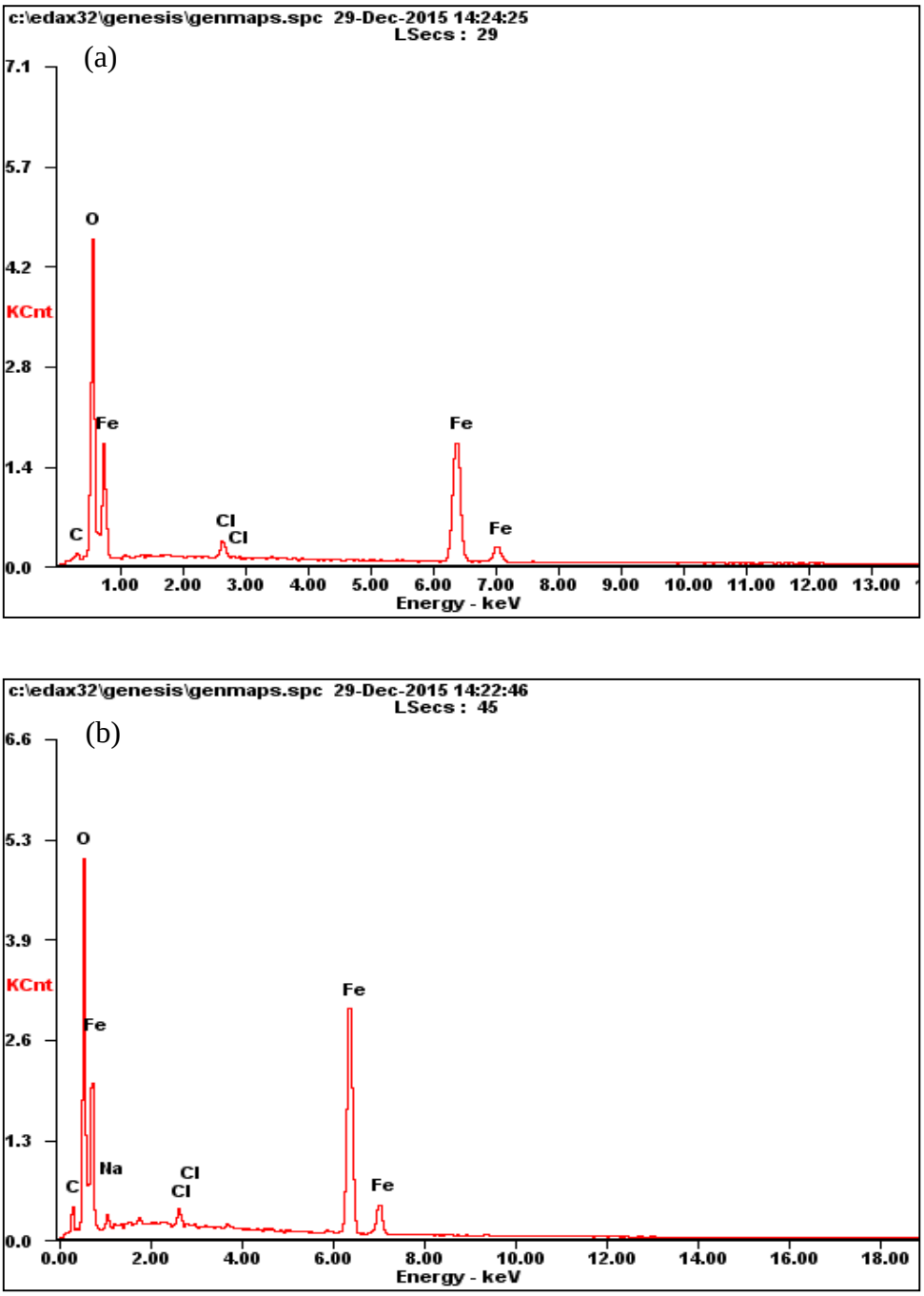

Figure 5. EDS analysis diagrams of the corrosion productions of the 20# carbon steel samples with different defect sizes after immersing in simulated solution for 10 days: (a) 200μm and (b) 800μm

Figure 5 is the EDS analysis diagrams of 20# carbon steel samples with defect sizes of 200μm and 800μm after immersing in simulated solution for 10 days. It can be seen from the figure that the content of Fe at the 200μm width defect is greater than that in the 800μm width defect. At the 200μm width defect, the corrosive ions in the solution continue to react with the 20# carbon steel substrate through the corrosion product film that covers the access to the defect; moreover, the above process forms a new corrosion production film. However, at the 800μm width defect, the thick corrosion product

film makes it more difficult for corrosive ions to continue to react with the 20# carbon steel substrate. The content of the new corrosion products is very small, and the content of Fe element is relatively lower.

3.2 LEIS measurement results and discussion

Figure 6 shows the LEIS surface measurement diagrams of 20# carbon steel samples with 200μm and 800μm width defects after immersing in simulated solution for 10 days. It can be seen from the figure that the impedance mode value of the coating defects in the whole scanning area decreases to the minimum as the distance from the defect increases. The area of the low impedance modulus in Figure 6 (b) is higher than that in Figure 6 (a), which is consistent with the influence of the coating defect sizes. The impedance mode values of defects with width of 200μm and 800μm are $1.8 \times 10^7\Omega$ and $1.7 \times 10^7\Omega$, respectively, and the former is higher than the latter.

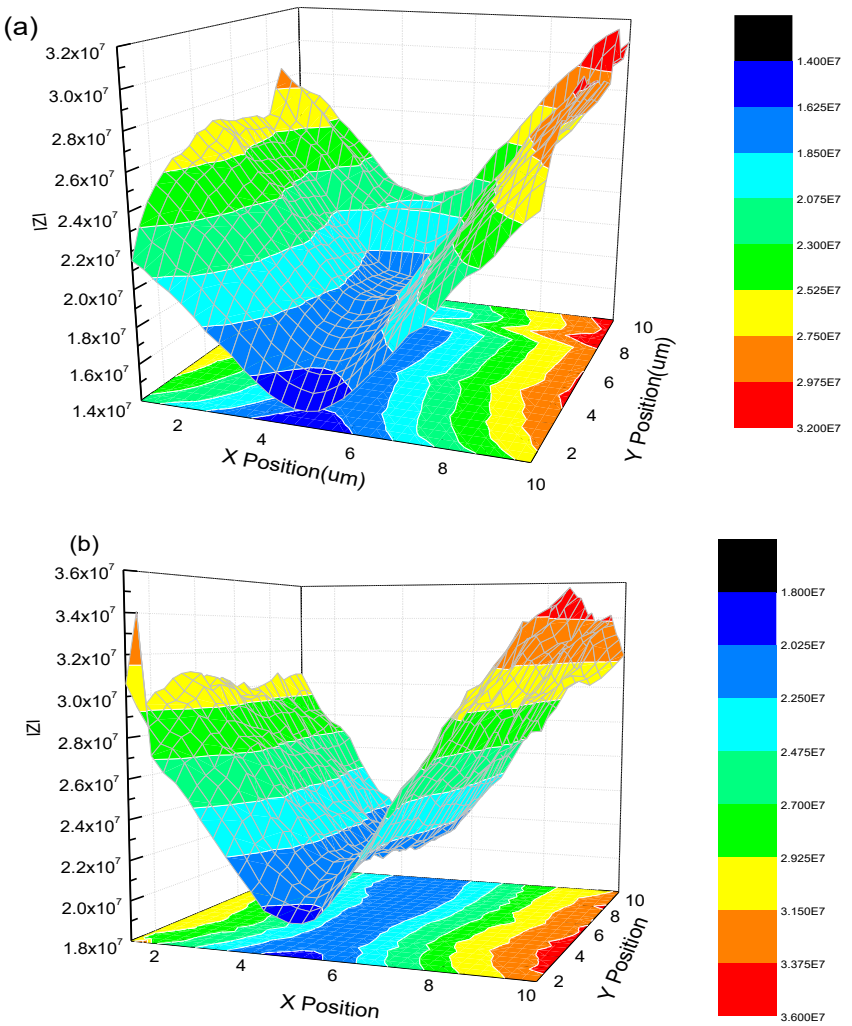

Figure 6. LEIS surface measurement diagrams of the 20# carbon steel samples with different defect sizes after immersing in simulated solution for 10 days: (a) 200μm and (b) 800μm

The metal substrate can be analyzed from the above results that at the coating defect after immersion in the solution and reacting with the corrosive ions in the simulated solution. The reaction formulations are as following:

Anode reaction: $Fe \rightarrow Fe^{2+}+2e$;

Cathode reaction: $O_2 + H_2O + 4e \rightarrow 4OH^-$

After a short time of the anode and cathodic reaction, the metal substrate inside the coating defect gradually dissolves, and the corrosion production content gradually increases. The corrosion productions are formed in the coating defect, which make it difficult for the oxygen outside the defect to diffuse to the inside of the defect, thus stopping the further reaction from continuing at the defect. Additionally, electrical transfer is blocked as the corrosion production film form on the collective surface of the metal inside the defect and the exposed surface of the defect; thus, crevice corrosion enters has entered the development stage. The metal substrate inside the defect underwent a series of reactions as following:

$$Fe + H_2O \rightarrow Fe(OH)_{ads} + H^+ + e$$

$$Fe(OH)_{ads} + H_2O \rightarrow Fe(OH)^+ + 2H^+ + 3e$$

$$Fe(OH)^+ + H^+ \rightarrow Fe^{2+} + H_2O$$

$$Fe^{2+} + SO_4^{2-} \rightarrow (FeSO_4)_{ads}$$

$$Fe^{2+} + Cl^- \rightarrow FeCl_2$$

$$(FeSO_4)_{ads} + SO_4^{2-} \rightarrow FeSO_4 + SO_4^{2-}$$

$$Fe^{2+} + HCO_3^- \rightarrow (FeCO_3)_{ads} + H^+$$

$$Fe^{2+} + 2H_2O \rightarrow Fe(OH)_2 + 2H^+$$

$$Fe(OH)_2 + HCO_3^- \rightarrow FeCO_3 + H_2O + OH^-$$

$$FeSO_4 + 2H_2O \rightarrow Fe(OH)_2 + 2H^+ + 2SO_4^{2-}$$

$$FeCl_2 + 2H_2O \rightarrow Fe(OH)_2 + 2H^+ + 2Cl^-$$

$$FeCO_3 + 3H_2O \rightarrow Fe(OH)_2 + 2H^+ + 2HCO_3^-$$

During the reaction process, acidification of the medium in the defect will lead to a decrease in the pH value inside the defect because the content of H^+ in the gap increases. The decrease in pH accelerates the further corrosion of the metal inside the defect, produces an autocatalytic effect in the occluded space, and finally lead to the complete destruction of the metal substrate. For the sample with 200μm defect width, due to its small defect size and the blocking effect of the corrosion production deposition, the metal substrate at the defect cannot react fully with the corrosive ions in solution, so the resistance of AC mode resistance is still high. In contrast, the sample with 800μm defect width shows a relatively open system and minimal blocking caused by corrosion products, the effect is not obvious and can even be ignored. After immersion in simulated solution, it can fully react with corrosive ions. Therefore, the AC impedance mode value of the 800μm width defect is lower than that of 200μm width defect.

The conclusion above is consistent with previous similar studies. Zhong [9] found that for small defect sizes which are less than 200μm in diameter, localized corrosion process and mechanism change with time. But for bigger defect sizes which are up to 1000μm, the LEIS responses measured at the defect are always featured by a coating impedance and the block effect of corrosion product does not apply due to the relatively open geometry associated with the big defect. Ma [20] studied pitting corrosion behaviors of copper with different grain sizes (23μm,67μm and 470μm) in different solutions

with EIS and found that the pitting susceptibility increased with increasing copper grain size, which was related to a decrease in the quality of the formed passive film. Godinez-Salomon [21] found that nanoparticles oxidize more easily when their size decreases. Song [22] researched failure process of waterborne coating/metal interface by LEIS and EIS and found that with the decreasing of defect size, the characteristics of the resistance of the coating changes from those of an interface corrosion reaction to those of an impedance with diffusion. As a small defect presents a relatively closed system, the failure process of the coating is blocked by the deposition of corrosion productions.

Figure 7 is the equivalent circuit fitting for LEIS which can be described by the expression R(Q(R(Q(RW)))).

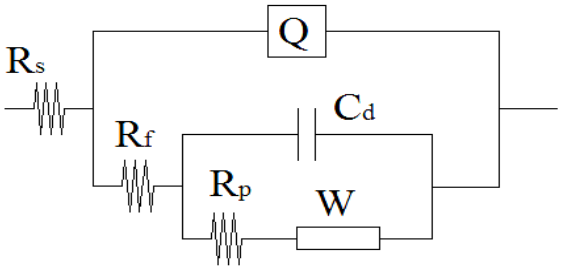

Figure 7. Equivalent circuit fitting LEIS for 20# carbon steel

The impedance expression of the above equivalent circuit is as following:

$$Z = Rs + \frac{1}{j\omega(Q) + \frac{1}{R_f + \frac{1}{R_{cd}} + j\omega C_d}} \quad (3)$$

Where R_S is the resistance of simulated solution, Q is the capacitance value of corrosion productions on the surface of the sample, R_f is the resistance of corrosion productions on the surface of the sample, C_d is the double layer capacitance of corrosion interface, and W is the charge transfer resistance.

Table 2. Dynamic parameters of LEIS of 20# carbon steel samples with different defect sizes after immersing in simulated solution for 10 days

Defect sizes	R_s ($\Omega \cdot cm^2$)	R_f ($\Omega \cdot cm^2$)	R_p ($\Omega \cdot cm^2$)	n
200 μm	46.02	220.6	1420	0.801
800 μm	25.04	1389	2596	0.885

The double electric layer between the electrode and the solution is generally represented by an equivalent capacitance, but due to the dispersion effect of the whole measurement system, the phase angle element (CPE) Q is often used instead of the capacitance element to characterize the influence of diffusion process on the electrode reaction. The impedance equation is as following:

$$Z_{CPE} = Y_0^{-1}（jw）^{-n} \quad (4)$$

Where parameter Y_0 represents the basic admittance value corresponding to CPE, and parameter n represents the index of dispersion effect size, whose value is generally between 0 and 1. The smaller the n value is, the greater the dispersion effect of the system is.

The results shown in Table 2 are obtained after fitting local impedance data of the equivalent circuit in Figure 7.

It is generally believed that R_f is related to the density of the corrosion production film. The higher R_f is, the higher the density of the corrosion production film is. In addition, the value of R_f increases with the defect size increases, indicating that the thickness of corrosion production film continues to increase with the extension of corrosion time, and the value of n indicates that the density of corrosion production film also increases gradually. The value of n in the table increases with the increase of defect size, indicating that when the defect size increases, the density of corrosion production film increases.

Figure 8 is the macro corrosion morphologies of the 20# carbon steel sample with different defect sizes after immersing in the simulated solution for 10 days. It can be observed that with the increase in defect size of the coating, the content of corrosion products in the defect area increases, and the distribution of the rust layer is more uniform. This is because the increase in the defect size of the coating leads to the opening of the reaction system. The reaction degree of 20# steel with corrosive ions in the solution at the 800μm width defect area is more sufficient. The reaction system at the 200μm width defect area of the coating is relatively occluded due to the size limitation and a more uniform corrosion production. The results show that the AC impedance mode of the 800μm width defect is lower than that of the 200μm width defect.

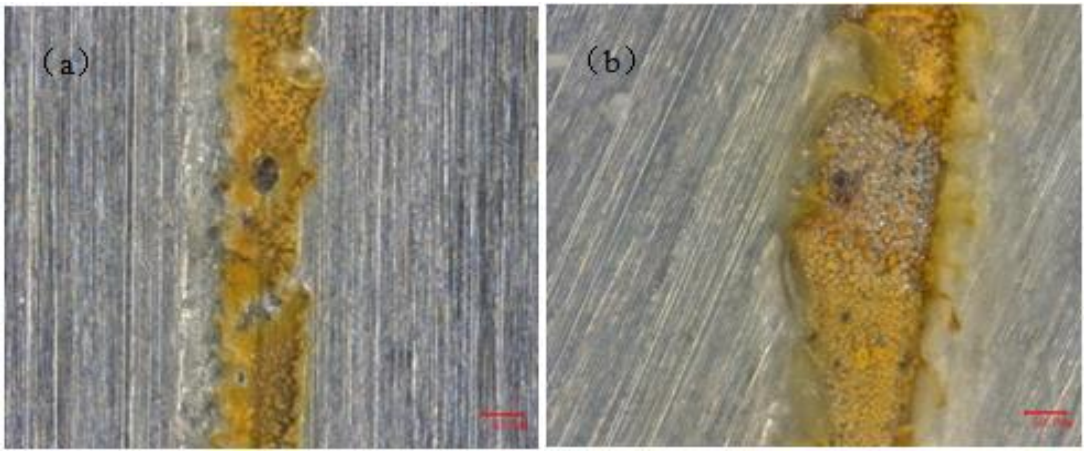

Figure 8. Macro corrosion morphologies of the 20# carbon steel samples with different defect sizes after immersing in simulated solution for 10 days: (a) 200μm, (b) 800μm

Figure 9 is the EDS analysis diagrams of the 20# carbon steel samples with 200μm and 800μm width defects after immersing in simulated solution for 10 days. It can be seen from the figure that the content of Fe in the corrosion productions generated at the defects of the 200μm width is lower than that

at the 800μm width defects, indicating that the reaction between the metal substrate and the corrosive ions in the solution is more sufficient at the 800μm width defects.

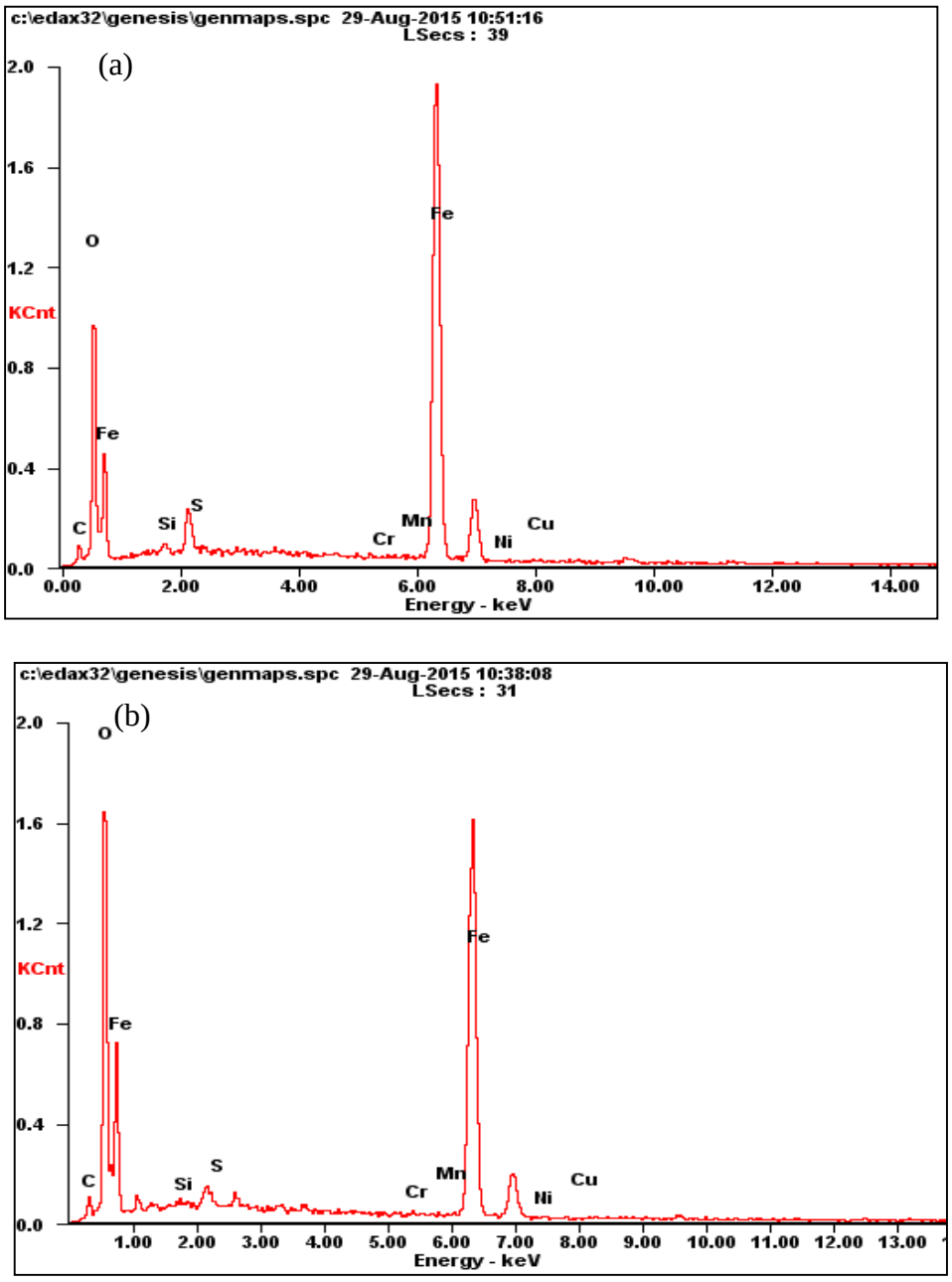

Figure 9. EDS analysis diagrams of 20# carbon steel samples with different defect sizes after immersing in simulated solution for 10 days: (a) 200μm and (b) 800μm

4. CONCLUSIONS

(1) The potential of defects with 200μm and 800μm width reached the maximum value after immersing in simulated solution for 10 days, which was 0.2500V and 0.0125V, respectively; the former

was higher than the latter. In addition, with an increase in the defect width, the overall potential of the defect shifted negatively; moreover, the surface potential tended to be uneven and gradually increased.

(2) The corrosion degree of the coating defects with different widths was different after immersion in the simulated solution, and the reaction between the metal substrate and the corrosive ions in the solution is more sufficient at the 800μm width defects. When the coating defect with the 200μm width was immersed in simulated solution, the local impedance mode value was higher than that of the 800μm width defect width.

References

1. M. Grund, T.W. Schmid and M. Stratmann, *Electrochim. Acta*., 45 (2000) 2515.
2. H. Sheng, C.F. Dong and K. Xiao, *Acta Metall. Sinica*., 4 (2012) 414.
3. A. Nazarov, T. Prosek and D. Thierry, *Electrochim. Acta*., 53 (2008) 7531.
4. W. Furbeth and M. Stratmannn, *Prog. Org. Coat*., 39 (2000) 23.
5. M. Doherty and J.M. Sykes, *Corros. Sci*., 46 (2004) 1265.
6. H.L. Yang, M. Zhang and A. Singh, *Int. J. Electrochem. Sci*., 13 (2018) 9131.
7. P. Yi, K. Xiao, C.F. Dong, K.K. Ding, M. Liu and X.G. Li, *Int. J. Electrochem. Sci*., 10 (2015) 7754.
8. Q.T. Jiang, X. Zhao, K. Zhang, X.G. Li, J. Zhang and B.R. Hou, *Int. J. Electrochem. Sci*., 12 (2017) 10199.
9. C. Zhong, X. Tang and Y. Cheng, *Electrochim. Acta*., 53 (2008) 740.
10. F. Zou and D. Thierry, *Electrochim. Acta*., 42 (1997) 293.
11. C.F. Dong, A.Q. Fu and X.G. Li, *Electrochim. Acta*., 54 (2008) 628.
12. Jorcin, J.B. Aragone and M. Cetal, *Corros. Sci*., 48 (2006) 1779.
13. T.T.X. Hang, T.A. Truc and T.H. Nam, *Surf. Coat. Technol*., 201 (2007) 7408.
14. Dehri, I. Howardrll and Tonsb, *Corros. Sci.*, 41 (1999) 141.
15. H.R. Zhou, W. Yao, C.W. Du, S.P. Song and R. Wu, *Int. J. Electrochem. Sci*., 12 (2017) 9542.
16. B. Losiewicz and J. Kubisztal, *Int. J. Hydrogen. Energy*., 43 (2018) 20004.
17. S.N. Wang, Y.H. Gu, Y.L. Geng, J. Liang, J. Zhao and J. Kang, *J. Alloys. Compd*., 826 (2020) 153976.
18. S. Trasatti and R. Parsons, *Pure Appl. Chem*., 58 (1986) 437.
19. A. Nazarov and D. Thierry, *Electrochim. Acta*., 52 (2007) 7689.
20. Y.H. Ma, X.X. Tian, J.F. Yin, J.P. Chen and J.N. Jiang, *Int. J. Electrochem. Sci*., 14 (2019) 4047.
21. G. Salomon, E. Estrada and M. Lopez, *Int. J. Electrochem. Sci.,* 7 (2012) 2566.
22. D.D. Song, H.X. Wan, X.H. Tu and W. Li, *Prog. Org. Coat*., 142 (2020) 105558.